21. STRESS-REGIME-CONTROLLED YIELD AND STRENGTH BEHAVIOR OF SEDIMENT FROM THE FRONTAL PART OF THE NANKAI ACCRETIONARY PRISM[1]

V. Feeser,[2] K. Moran,[3] and W. Brückmann[4]

ABSTRACT

Sediments undergoing accretion in trench-forearc systems are subjected to conditions of large lateral thrusting. This stress regime controls the mechanism of faulting as well as the yield and strength properties of the sediment. Understanding them is therefore crucial for the construction of quantitative models of sediment dynamics in convergent margin settings.

For this purpose triaxial and oedometer tests were performed on six whole-round core samples recovered from Site 808 from depths between 173 and 705 mbsf. Samples from five depth intervals were subjected to a triaxial test program that was primarily designed to define yield and strength behavior. Test specimens were cut parallel and normal to the core axis. Additional five oedometer tests with similarly prepared specimens were performed on samples from four depth intervals to evaluate the directional state and degree of sediment compaction.

Test results show that the degree of sediment compaction is higher than expected from overburden. This overcompaction increases with depth. A well-developed mechanical anisotropy is evident in all samples tested, regardless of their depth and lithology. Values of yield limit, stiffness, and shear strength are up to 40% higher in the horizontal direction compared to the vertical direction. In addition the test data demonstrate that the axis of the volumetric yield loci have rotated into extensional stress field. This verifies that the mechanical state of sediment in the accretionary wedge is controlled by in-situ stress conditions of extensional nature. The coefficients of lateral stress inferred suggest that the extensional stress regime becomes increasingly effective with depth.

INTRODUCTION

Leg 131 was dedicated to the study of the Nankai Trough accretionary wedge, which represents a typical example of convergent margins characterized by a high input of clastic sediment. This is the most frequently occurring type among the circum-pacific plate boundaries. The working area (Fig. 1) is characterized by a regular tectonic style of imbricate thrusting and sediment deformation, making it an ideal choice for the evaluation of problems relevant to convergent margins in general. Studies on the interdependency of deformational processes, physical properties, structural development, and hydrology in accreting and accreted sediment were among the most important goals of this cruise. Many of these objectives could be accomplished by drilling Site 808 in the frontal part of the toe of the accretionary wedge (Taira et al., 1991), which provided a continuous profile through the accretionary sequence, the décollement, and the subducting sequence at the deformation front of an active accretionary prism (Fig. 2). One of the most remarkable features of Site 808 is the strong dichotomy in structural styles and downhole physical property trends above and below the décollement. Many deformational structures covering a wide range of scales were found between frontal thrust and décollement, reflecting the compressional tectonic regime in the frontal deformation zone of the prism. Below the décollement virtually no signs of deformation could be detected, indicating the complete mechanical decoupling between the accreting and the subducting portion of the sedimentary sequence.

The formation and development of accretionary wedges at convergent margin settings are controlled by the mechanical properties of the sediments accreted. Furthermore, these properties are strongly influenced by the actual stress regime to which these sediments are subjected. Therefore, the interpretation of accretionary faulting mechanism requires knowledge of the sediment yield and strength behavior as well as of the in-situ principle stress state. Accurate stress values, however, could be only obtained by in-situ measurements in boreholes. Owing to the complicated testing techniques necessary to obtain reliable in-situ data, only a few successful attempts have been made in ODP holes (Moran et al., this volume). Therefore, an insight into the in-situ stress conditions, usually, has to be indirectly estimated from stress-strain properties from laboratory tests on undisturbed samples.

In this paper experimental data from one-dimensional consolidation tests and triaxial shear tests performed on whole-round core samples from Leg 131 were used to obtain an insight into the general in-situ principle stress state of the Nankai Trough trench-forearc system and to investigate how the yield and strength properties of the accretionary wedge sediments is influenced by this stress regime.

CONCEPTS

One-dimensional Consolidation

The pattern of stresses within a sediment mass is described by the ratio of horizontal to vertical effective principle stress and is expressed by the factor K, called the coefficient of lateral stress:

$$K = \frac{\sigma'_h}{\sigma'_v} .$$

Sediments with horizontal surfaces deposited over areas of large lateral extent where there has been no lateral strain are subjected to principle geostatic stress states with major stresses in the vertical and minor stresses in the horizontal direction. In this special case, the stress ratio is called the coefficient of lateral stress at rest, and is denoted by the symbol K_0. During deposition with monotonously increasing overburden each state of stress of a soil element will be essentially similar to all preceding states. Therefore, the value of K_0
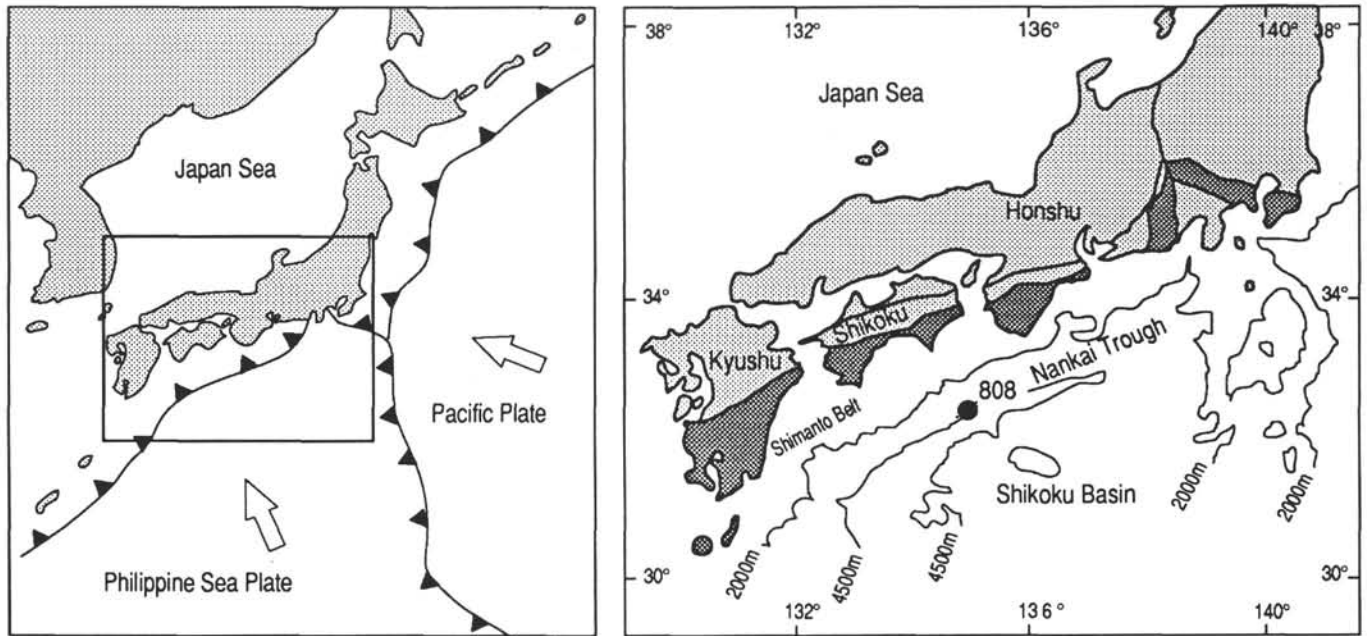
Figure 1. Plate boundaries and geotectonic reference frames around Japan and location map of the Site 808 working area in the Nankai Trough accretionary complex.

is found to be a constant (K_0-line, Fig. 3A). The coefficient of lateral stress at rest can be usually approximated by:

$$K_0 = 1 - \sin \varphi' ,$$

where ϕ' is the effective friction angle (e.g., Das 1985).

For sediments in geostatic stress states, symmetry dictates that the individual soil particles can only move downward during the consolidation. Therefore, the process of compaction is entirely one-dimensional and can be plotted in a compression plane of vertical effective stress $\sigma v'$ vs. deformation, i.e., void ratio e, vertical strain ε_v, or specific sediment volume V (branch AB, Fig. 3B).

If the sediment is unloaded, the stress-deformation response will show an unloading curve BC (Figs. 3A, 3B) causing a permanent plastic deformation. On reloading from C, the path is nearly retraced to point B where the virgin curve AB is subsequently extended. The point B indicates yield of the sediment for the reloading cycle CE. In the phase BE, the material is undergoing plastic strain-hardening again during which a new yield condition is created (Figs. 3A, 3B). In this context a sediment is called normally consolidated (NC state) if the present vertical geostatic stress σ_v' is the maximum to which the sediment has ever been subjected. An overconsolidated sediment (OC state) will occur if the present overburden stress σ_v' is less than the maximum to which the sediment has ever been subjected (Fig. 3B).

Distinct information on the state of consolidation of a sediment will be received by analyzing the stress-strain behavior, from which one obtains the sediment stiffness or tangent modulus M, defined as:

$$M = \frac{d\sigma'_v}{d\varepsilon'_v} .$$

During geostatical normal consolidation the sediment stiffness and the modulus M, respectively, increases linearly (branch AB, Fig. 3C). Unloading from B to C leads to a further, yet non-linear, increase in the stiffness. During reloading, M increases up to a peak value at point D, whereafter it decreases until the preconsolidation stress level B is reached. By further loading in the phase BE the sediment reacts as normally consolidated again with a linear increase in M. In most cases

the peak of the reloading branch (point D) marks the actual overburden stress $\sigma_{v\,act}'$ (Janbu et al., 1981). Due to the marked change in sediment stiffness passing the over/normal-consolidation transition the preconsolidation stress level can be generally reconstructed better by an σ_v' vs. M plot (Fig. 3C) than by the conventional methods (e.g., Casagrande 1936) using the σ_v' vs. e plot (Fig. 3B).

It has been suggested that normally consolidated sediment (branch AB, path 1, Fig. 4A) in trench-forearc systems become overconsolidated not by increasing overburden, but through increasing horizontal stress σ_h' caused by conditions of large lateral thrusting (branch BC, path 2, Fig. 4A). This type of loading is called extensional due to resulting extensional deformation in vertical direction. Although, there is no or only a minor change in the effective overburden stress σ_v' the void ratio e is decreased by the extensional loading (Fig. 4B).

Point C represents the actual in-situ state of the sediment. In this case the coefficient of lateral stress K does not correspond any longer to K_0 and to the friction angle ϕ', K may be expected to range to unity or higher (Fig. 4A). This expression of overconsolidation is reflected in the σ_v' vs. e plot as well. Point C lies beneath the virgin consolidation line.

If a sample is taken from this state, stress release will produce a swelling curve CD. If the sample is subsequently geostatically reloaded in the laboratory, a response curve DF will be obtained as shown in the plots of Figures 4A, 4B, and 4C. Comparing the three individual branches of the reloading curve, it is evident that σ_v' vs. M plot (Fig. 4C) provides the most distinct information on the state of consolidation. As mentioned above, the peak value of sediment stiffness at point E indicates the actual effective vertical overburden stress $\sigma_{v\,act}'$. In the case of accretionary thrusting this stress state usually corresponds with the maximum vertical preconsolidation stress to which the sediment has ever been subjected. The abrupt change in the tangent modulus at point F is not connected with the maximum overburden stress but indicates the new yield point caused by horizontal accretionary thrusting. This stress state might be termed vertical imaginary preconsolidation stress $\sigma_{v\,im}'$.

According to the overconsolidation ratio OCR used to describe the degree of vertical overconsolidation (e.g., Das 1985), the ratio of the vertical imaginary preconsolidation stress $\sigma_{v\,im}'$ and the vertical actual overburden stress $\sigma_{v\,act}'$, named overloading ratio OLR to express the
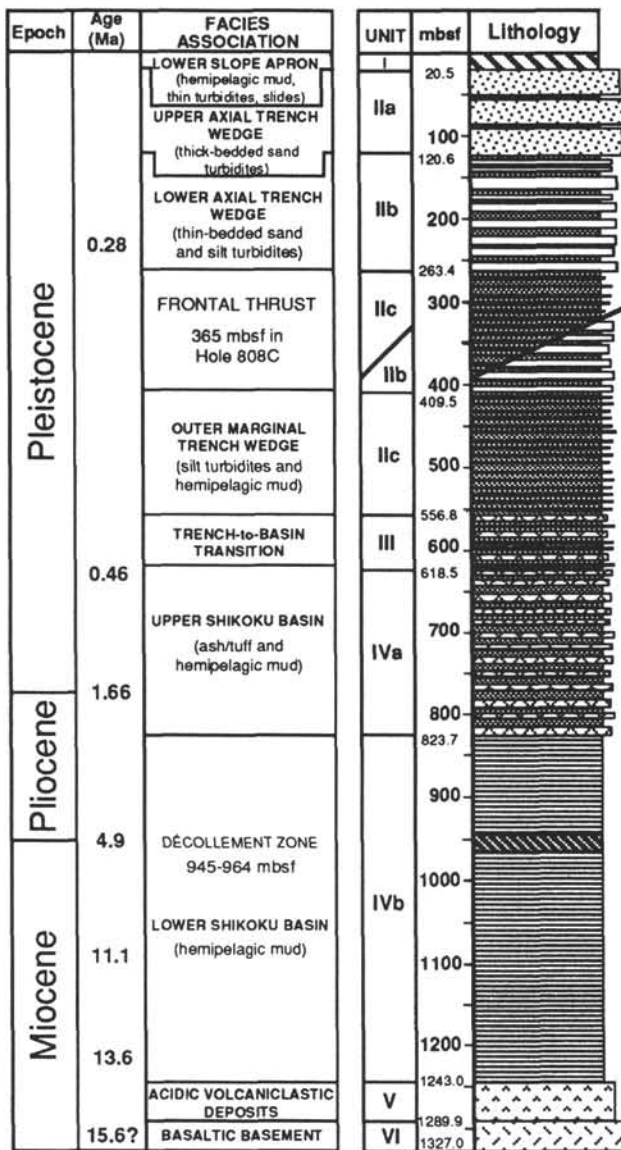
Figure 2. Chronostratigraphy and lithofacies profile of Site 808.

$$p' = (\sigma'_a + 2\sigma'_r)/3$$

as mean effective stress and

$$q = \sigma'_a - \sigma'_r$$

as deviator stress are used, where σ'_a denotes the effective axial and σ'_r the effective radial stress measured in triaxial testing, which correspond with the effective vertical and effective horizontal in-situ stress.

It has been found that geostatic loading creates volumetric yield loci (YL 1, YL 2) as shown in Figure 5 (Parry and Nadakajah, 1974). The shape of these loci is found to be nearly elliptical and mostly symmetrical to the K_0-line (Graham et al., 1983). Stress changes within a yield locus (e.g., YL 1, path AB, Fig. 5) are accompanied by purely elastic or recoverable deformations. Stress changes outside the yield locus will cause the sediment to yield. Irrespective of the direction of the stress change, the original yield locus is expanded to a new current yield surface (YL 2, paths AC, AD, AE, Fig. 5). This subsequent yield locus will still have the same elliptical shape centered on the K_0-line if the changes in stress ratio remain minor. If the sediment is subjected to a large increase in effective stress, deviating from previous loading (path AF, Fig. 5), the subsequent yield locus YL 3 will show recognition of the new stress ratio. The hardening of the soil, i.e., the expansion of the elastic region, would have occurred preferentially in the direction of the new loading (Wood 1990). The shape and orientation of the new yield locus YL 3 will still remain elliptical and centered on the loading stress path AF (Fig. 5).

A typical yield locus for sediment that has undergone large extensional loading after geostatic compression as occurs within accretionary settings (path 1–2, Figs. 4A, 6) might have a shape shown in Figure 6. Consequently, a sample of this sediment tested under undrained triaxial conditions would show different responses in yielding, depending on whether the deviator stress is increased (compression test, path AC, Fig. 6) or decreased (extension test, path AE, Fig. 6). In the case of compression, the elastic response (path AB) would be less than in extension (path AD). Therefore, on the assumption that the actual in-situ stress state must be located on the extensional loading path 2 and on the basis of yield data obtained from triaxial compression and extension tests as well as from oedometer tests, the in-situ stress conditions could be generally reconstructed by the graphical procedure as outlined in Figure 6.

METHODS

Oedometer Tests

The apparatus used for one-dimensional consolidation tests was a fixed-ring oedometer with drainage at the top and bottom of the sample. The dimension of the samples was 16 mm in height and 31 mm in diameter. The loading of the sample was applied through a mechanical lever arm up to 10 MPa and the settlement was measured with an LVDT. The specimen was kept under water after reconsolidation up to the calculated in-situ overburden stress. The test were performed according to the IL EOP-method (incrementally loading after end of primary consolidation) as recommended by Mesri and Choi (1985).

Triaxial Tests

A modernized triaxial device of the type developed at the Institute for Soil Mechanics at Karlsruhe University, was used (Topolnicki, 1987). This device complies with the standards according to the suggestion of Berre (1985). It has been equipped with a microcomputer for data acquisition, control operations, and processing of the sample data. The general layout of the apparatus is shown in Figure 7.

Test specimens with an initial ratio of height to diameter $H_0/D_0 = 1$ were used instead of the commonly practiced ratio of 2. This is because it has been observed that short specimens deform more homogeneously
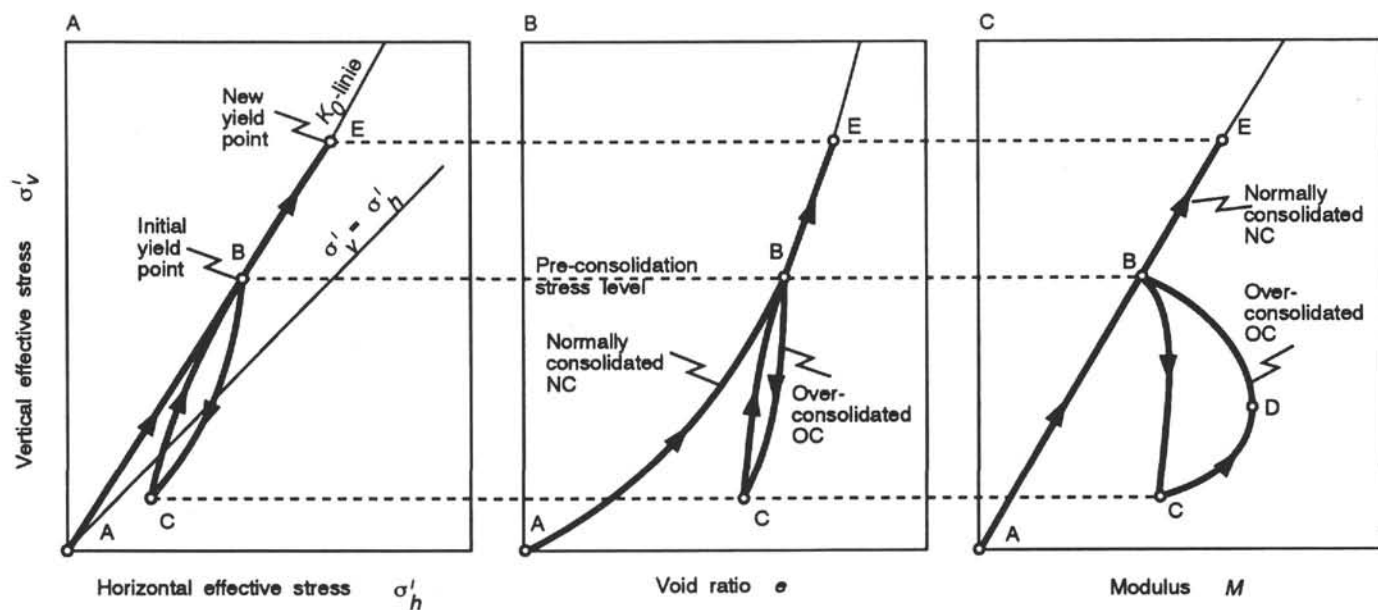
distinct origin of sediment deformation, could be employed to quantify the degree of compaction by an additionally extensional loading:

$$\text{OLR} = \frac{\sigma'_{v\ im}}{\sigma'_{v\ act}}$$

Until now, there is a lack of information on the influence of the stress-deformation history on the magnitude of experimentally determined values of the maximum overburden stress as well as the imaginary preconsolidation stress. Thus, the data of the imaginary preconsolidation stress and the actual overburden stress experimentally obtained can only give qualitative information on the magnitude of the actual horizontal stress state.

Shear Deformation Behavior

In the previous section, yielding, i.e., plastic volumetric deformation, has been associated with single points in the principle stress plane (Figs. 3A, 4A). These yield relations should be extended to general shear deformation behavior. Therefore, the generalized stress components (Cambridge invariantes, Roscoe et al., 1958)

Figure 3. Mechanical behavior of sediment undergoing one-dimensional consolidation under virgin, unloading, and reloading conditions. **A.** Principle stress field. **B.** Arithmetic plot of effective overburden stress vs. void ratio. **C.** Development of sediment stiffness.
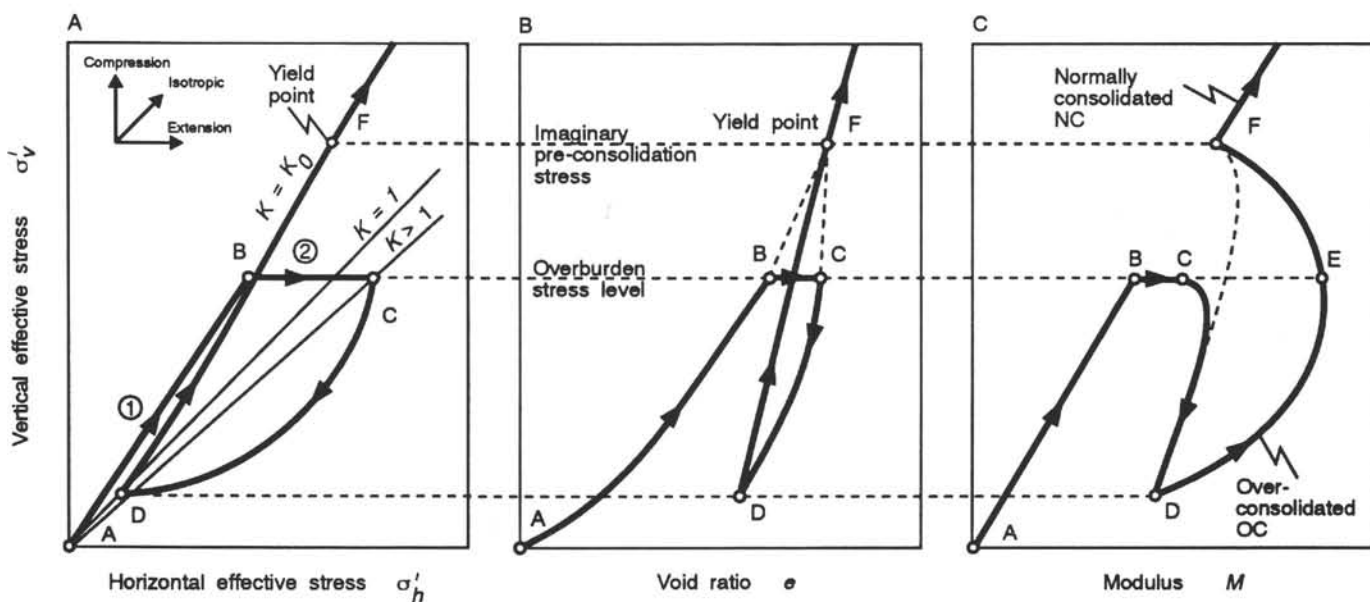

Figure 4. Influence of directional lateral loading superimposed on one-dimensional consolidation of sediment. **A.** Principle stress field. **B.** Arithmetic plot of effective overburden stress vs. void ratio. **C.** Development of sediment stiffness.

than specimens with a lower height-to-diameter ratio (Vardoulakis, 1979). Hence, this practice makes good lubrication of the end platen necessary. This was obtained by lubricating the loading pedestals and covering them with a circular latex disc. Two latex membranes were placed around the sample with a lubrication between them. Pore-pressure measurements and drainage were allowed by a filter of 10 mm diameter in the bottom platen.

Saturation of the specimen was achieved by applying back pressure prior to the reconsolidation. The reconsolidation was performed isotopically up to or slightly above the calculated in-situ overburden stress. After that, the specimens were loaded undrained and sheared to failure (CIUC test). Excess pore pressure was measured. Because the pore pressure is governed by the volumetric strain characteristics, the yield point could be estimated by a sharp increase in pore pressure.

The triaxial apparatus employed did not allow the application of vertical extension tests. However, to obtain information on vertical extension stress-strain behavior, triaxial specimens were cut normal to the core axis and were loaded axially by compression according to the common test procedure. With that approach vertical extension tests could be sufficiently approximated. Thus, in the following, triaxial tests on specimens loaded normal to core axis will be denoted as extension tests.

To mark the individual tests, a combination of an abbreviation of the test type (OE = oedometer test, TR = triaxial test), the numerical ODP sample identifier and an extension (V, H) denoting the orientation of the axis of the test cylinders is used. So, the notation OE 808G-8X-4 (H) marks an oedometer test, done on a specimen cut normal to the core axis from Section 808G-8X-4.
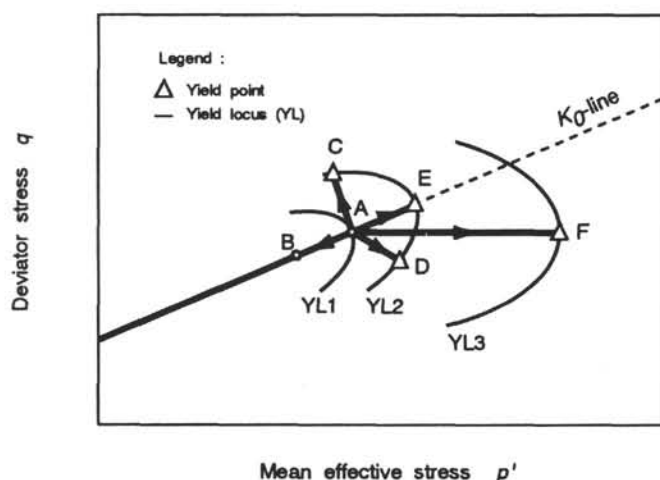
Figure 5. Stress path producing recoverable and irrecoverable changes in volume. Expansions of initial yield locus YL 1 to YL 2 due to minor stress changes. Expansion and rotation of initial yield locus YL 1 to YL 3 due to large stress increase deviating from previous loading path.

An overview on all details of the oedometer and triaxial testing program is given in Table 1.

INDEX PHYSICAL PROPERTIES

Shipboard Data

All mass physical properties display an irregular downhole profile with major discontinuities across the frontal thrust and the décollement. While offsets occurring across the frontal thrust can be explained by the stratigraphic repetition of ca. 160 m, a fundamentally different genetic origin has to be assumed for the décollement. Between frontal thrust and décollement porosity, bulk density and water content show steady—albeit lithologically modulated—downhole trends, compatible with a normally consolidated to slightly overconsolidated state of the accreting sediments. The narrow (20-m wide) décollement zone itself is characterized by brittlely deformed, hardened sediments of low porosity and high density. Below the décollement another strong offset to higher porosity and lower density sediment marks the top of the subducting sequence. It has been suggested that an impermeable or overpressured décollement restricts dewatering of this sequence, causing high excess pore pressures and underconsolidation. This model is in good agreement with porosity and density profiles within the subducting sediments. All physical properties are discussed in detail in Taira et al. (1991).

Shore-based Data

In addition to standard shipboard index physical properties, we have determined Atterberg limits (liquid limit, plastic limit) and grain-size distribution data according to standard procedures as outlined in DIN 18122 (1967) and DIN 18123 (1983), respectively. Supplementary to the index tests, scanning electron micrograph (SEM) observations were made on the samples tested for qualitative sediment description. According to the suggestions of Barden and Sides (1971) the samples for SEM studies were cleaved from air-dried specimens. The exposure planes are oriented parallel to the core axis.

Results of these shore-based procedures are compiled in Table 2 and Figure 8. Based on these data, a threefold division of the sediments investigated is evident, which corresponds rather more to the lithological units than to the physical property units defined during Leg 131 for Site 808 sediments. According to Casagrande's plasticity chart classification system (1948) the Samples 131-808B-7X-3, 120–140 cm, and 131-808G-8X-4, 129–144 cm, of thin bedded sands
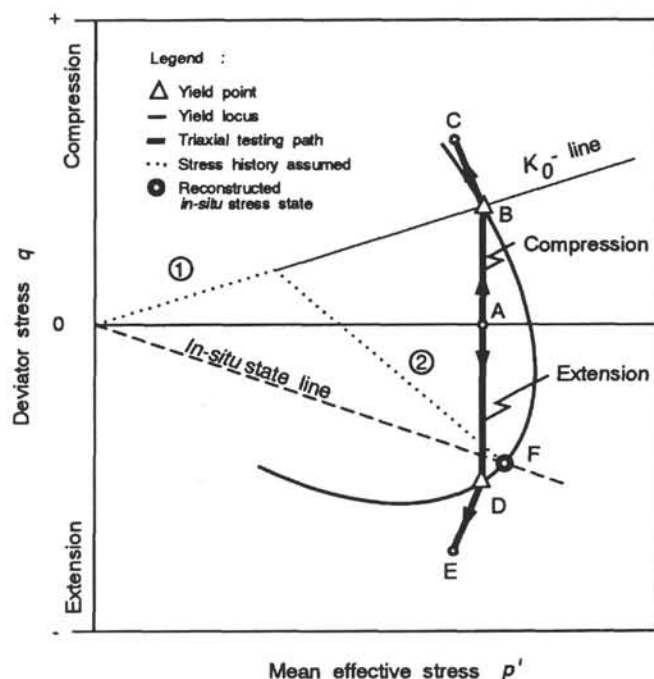

Figure 6. Graphical estimation of in-situ stress states of sediment that have undergone large extensional loading after geostatic compression (path 1–2) with the aid of a yield locus reconstructed from undrained triaxial compression and extension tests.

and silt turbidities from lithological Unit IIb (Lower Axial Trench Wedge, reference Fig. 2) are to be assigned as silts with lower plasticity. The silt turbidities and hemipelagic muds of the Samples 131-808C-17R-5, 19–29 cm, and 131-808C-23R-3, 2–14 cm, from lithological Unit IIc (Outer Marginal Trench Wedge, reference Fig. 2) show a geotechnical character of clays with medium plasticity. In contrast to sediments of Unit IIc, the Samples 131-808C-39R-5, 56–69 cm, and 131-808C-43R-2, 18–31 cm, of hemipelagic muds, ashs, and tuffs from Unit IVa (Upper Shikoku Basin, reference Fig. 2), on shipboard both joined to physical property Unit 3, have to be classified as clays of high plasticity.

All SEM observations supported this geotechnical characterization. As shown in Figure 8A, sediments from lithological Unit IIb consist primarily of well-sorted, very angular silt-sized particles. Sediments from lithological Unit IIc (Fig. 8B) are already more fine-grained than the former, but still show a high portion of angular silty particles. In agreement with the shore-based index properties, sediments from lithological Unit IIc differ from those of lithological Unit IVa which show a homogenous clayey matrix (Fig. 8C).

RESULTS

Oedometer Tests

The results from oedometer tests are presented as semi-logarithmic plots of void ratio e vs. vertical effective stress σ_v' (Fig. 9) and as plots of tangent modulus M vs. vertical effective stress σ_v' (Fig. 10). Parameters characterizing the compression and swelling behavior as well as the actual state of compaction, i.e., C_c, C_s, $\sigma_{v\ act}'$, $\sigma_{v\ im}'$, and OLR are presented in Table 3.

Due to instrumental limitations, samples could be subjected to a maximum vertical loading of 10 MPa. Therefore, only samples from depths down to 200 mbsf could be completely evaluated for their compression (NC state) and extension (OC state) behavior (Figs. 9A, 9B). Samples from greater depths did not reach the NC state. Thus, these samples yield reliable information on their swelling properties in the OC state only (Figs. 9C, 9D).
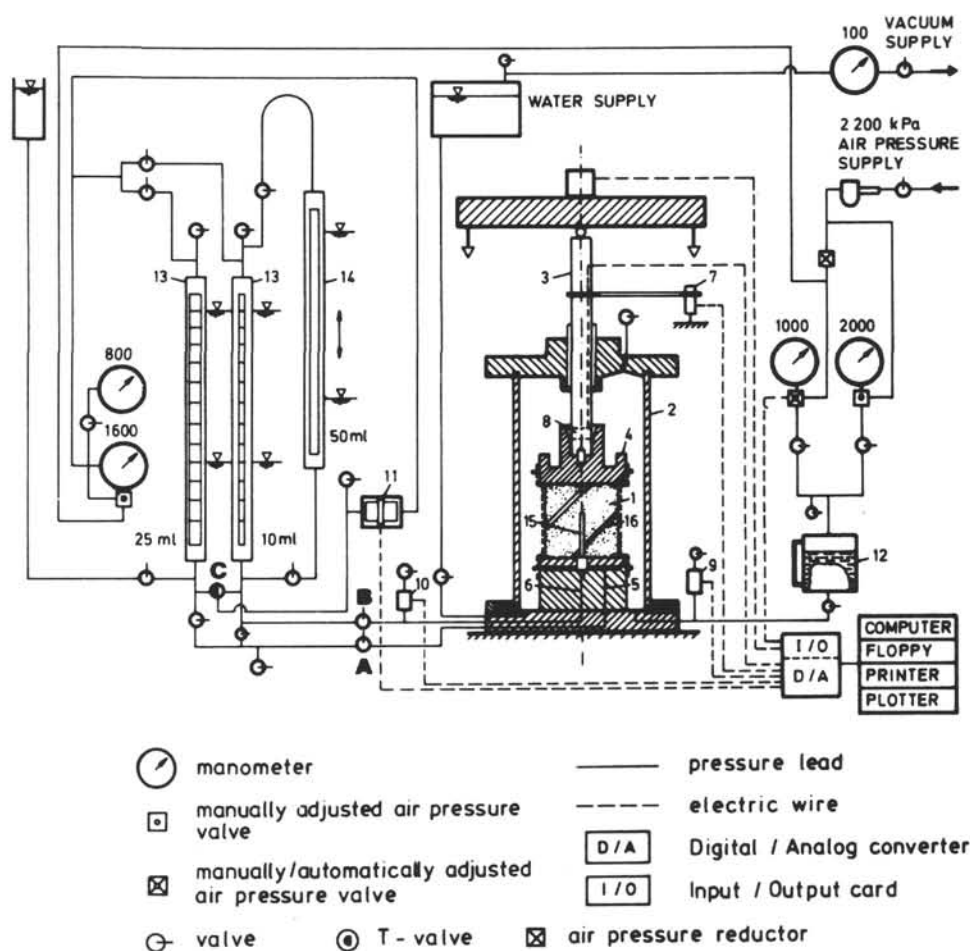
265

Figure 7. General layout of the triaxial apparatus used. 1, specimen; 2, triaxial cell; 3, loading piston; 4, loading cap; 5, drainage lead; 6, pore-pressure lead; 7, axial strain transducer; 8, strain gauge for axial load; 9, cell pressure transducer; 10, pore pressure transducer; 11, differential pressure transducer; 12, pressure cylinder; 13, fixed burettes; 14, movable burettes; 15, perforated pore pressure probe; 16, filter paper strips (from Topolnicki, 1987).

Table 1. Testing program.

Lithological units	Physical property units	Sample Hole	Sample Core, section	Sample Interval (cm)	Sample Quality	Depth (mbsf)	Vertical effective stress (cal.) (MPa)	Sample orientation (horizontal or vertical)	Reconsolidation stress (MPa)	Back pressure (MPa)	Strain rates (10⁻³ min⁻¹)	Oedometer tests Max. loading (MPa)
IIb	1	808B	7X-3	120–140	–	173.0	1.48	H	2.0	0.60	5/0.5/0.05	
								V	2.0	0.60	5/0.5/0.05	9.90
		808G	8X-2		±	194.5	1.61	V	0.80	0.40	8.3	
			8X-4	129–141	±	198.7	1.69	H				9.99
								V				9.99
IIc	3	808B	17X-3		±	266.4	2.28	V	1.49	0.40	8.3	
		808C	6R-2		±	348.9	3.02	V	0.40	0.40	8.3	
			17R-5	19–29	–	458.3	4.33	H	4.3	0.75	5/0.5/0.05	
								V	4.3	0.75	5/0.5/0.05	
			23R-3	2–14	±	514.0	4.89	V	4.8	0.75	5/0.5/0.05	9.99
IVa			39R-5	56–69	–	671.2	6.49	V	6.5/8.5	0.75	0.25	
					±			V	6.5/8.5	0.75	0.25	9.99
			43R-2	18–31	–	704.9	6.85	V	3.4/6.85	0.75	0.25	
					–			V	3.4/6.85	0.75	0.25	

Table 2. Soil mechanical index characterization of sediment from Site 808.

Sample			Atterberg limits[a]			Grain size distribution							
						Median M_d (mm)	Quartile (mm)		Clay (%)	Silt (%)			Sand (%)
Hole, core, section	Interval (cm)	Lithological units	w_L (%)	w_P (%)	I_P (%)		Q_1	Q_3		f	m	c	
808B-7X-3	120–122	IIb	46.5	28.3	18.2	0.0120	0.0035	0.030	20	16	30	20	14
808C-8X-4	129–130		46.2	31.9	14.3	0.0150	0.0035	0.050	19	14	25	22	20
808C-17R-5	19–29	IIc	58.3	30.6	27.7	0.0100	0.0024	0.045	22	19	24	13	14
808C-23R-3	2–14		62.0	31.0	31.0	0.0075	0.0024	0.030	22	24	25	11	20
808C-39R-5	68–69	IVa	69.3	23.3	46.0	0.0026	0.0010	0.010	44	22	18	6	10
808C-43R-2	18–20		88.4	23.0	65.4	0.0020	0.0004	0.014	45	17	17	10	11

[a] w_L = liquid limit; w_P = plastic limit; I_P = plasticity index.

Values of compression and swelling index derived from the oedometer curves are in the normal range (Table 3). It is remarkable that silts from a shallow section (Sample 131-808B-7X-3, 120–140 cm) with a low plasticity compared to clays with higher plasticity deeper in the Site 808 show a relatively high compression and swelling potential. This could indicate that sediments in Section 131-808C-39R-4 have already experienced a certain degree of cementation. This interpretation is supported by the observation that only low plasticity silts from shallower samples showed signs of relaxation (between sampling and testing), while samples with higher plasticity from deeper in the section did not (Fig. 9). The relaxation was anisotropic, due to the confining of the core liner about 30% less in horizontal than vertical direction. Appropriately the sediment showed a lower settlement in horizontal direction during the reloading phase (OC state) compared to the vertical direction. However, this anisotropic behavior can be subsequently traced in the NC region; thus, it is evident that the compressional anisotropy is an inherent sediment property rather than one induced by sample handling procedures.

This anisotropic sediment property is also documented in the behavior of sediment stiffness (Fig. 10). Patterns of test curves in this plot underline the already noted observation that only tests on the Samples 131-808B-7X-3, 120–140 cm, and 131-808G-8X4, 129–141 cm, reach NC state (Figs. 10A, 10B). This is indicated by a linear development of the stiffness lines that extend backward into the origin (dotted line in Figs. 10 A, 10B). The stiffness anisotropy of Sample 131-808G-8X-4, 129–141 cm, evidently extends over the whole loading range tested, with tangent modulus M being an average of 25% higher in the horizontal direction compared to the vertical direction.

As depicted in the concept section, the display of the development of sediment stiffness also yields information on the state and degree of compaction. The curve maxima in the lower stress region indicate the current overburden stress σ_{act}'. Comparing overburden stress values obtained by this way with values calculated from sediment density and height of the overburden column, a good agreement can be stated of both approaches (Table 3). The minima of stiffness curves consequently following the maxima were termed imaginary preconsolidation stress $\sigma_{v\,im}'$. They indicate the yield limit at the transition from the OC state to the NC state. As shown in Figure 10, this state could experimentally be defined in all samples except for Samples 131-808C-39R-5, 56–69 cm.

Imaginary preconsolidation stress and overburden stress are used to calculate overloading ratio OLR, which is an indicator for the amount of additional compaction the sediment has experienced due to imbricate thrusting in this part of the accretionary wedge. The clear increase of the OLR with depth shows the growing impact of accretion related to compaction with depth (Table 3). Although no OLR value could be calculated for Sample 131-808C-39R-5, 56–69 cm, the pattern of the stiffness line measured (Fig. 10D) also suggests a continuation of the trend of increasing impact to greater depths.

The impact of lateral stress greater the vertical geostatic loading is nicely shown through OLR values of tests OE 808G-8X-4 (V) and OE 808G-8X-4 (H) (Table 3): the horizontally loaded sample yielded an overloading ratio of 1.64, which is a factor 1.4 higher than the overloading ratio for the vertically loaded counterpart.

Triaxial Tests

Test results are presented as stress paths in q-p' space and pore pressure behavior as a function of deviatoric stress (Fig. 11); the inferred angles of internal friction are shown in Table 4.

As expected, the compressive strength increases with increasing depth, i.e., with increasing compaction, regardless of lithologic composition. Nevertheless, lithologic composition can exert a discernible influence on the straining process. A general difference in failure mechanisms in the post failure state can be observed between lithologic Units IIb on one side and Units IIc and IVa on the other side. Low plasticity silts of Sample 131-808B-7X-3, 120–140 cm, show strain-hardening in compressional as well as extensional tests (Fig. 11A), while higher plasticity clays from samples deeper in the site show post-failure strain softening (Figs. 11B, 11C).

Another remarkable feature is the difference in deviator stresses of yield points, which in both extensional tests TR 808B-7X-3 (H) and TR 808C-17R-5 (H) are 20%–40% higher than in the compressional tests TR 808B-7X-3 (V) and TR 808C-17R-5 (V) (Figs. 11A, 11B). This is in good agreement with the observation from oedometer tests OE 808G-8X-4 (V) and OE 808G-8X-4 (H) that the yield limit is about 20% higher in horizontal compared to vertical direction (Fig. 9B and Table 3).

The generally higher sediment stiffness in the horizontal direction is also well documented in the pore pressure development during shearing. In the initial phase of the extensional tests TR 808B-7X-3 (H) and TR 808C-17-5 (H) no or only minor change in pore pressure appears below the yield limit, indicating a high degree of stiffness caused by a horizontal preloading. The compression tests TR 808B-7X-3 (V) and TR 808C-17R-5 (V) on the other hand showed a steady increase in pore pressure during shearing. Interestingly the amount of the diagnosed stiffness anisotropy is identical in both samples regardless of their differing lithology.

The small number of whole-round core samples available made it impossible to define shear strength parameters for OC states. Therefore, all tests were run with reconsolidation stresses equal or above the in-situ overburden stress. The results deduced from these tests, i.e., the angles of internal friction, are therefore restricted to NC states. Furthermore, due to the relatively small number of tests it was not possible to define shear strength for single sections. However, the shear behavior observed within the individual lithological units make it possible to evaluate strength parameters for each lithological unit in Site 808.
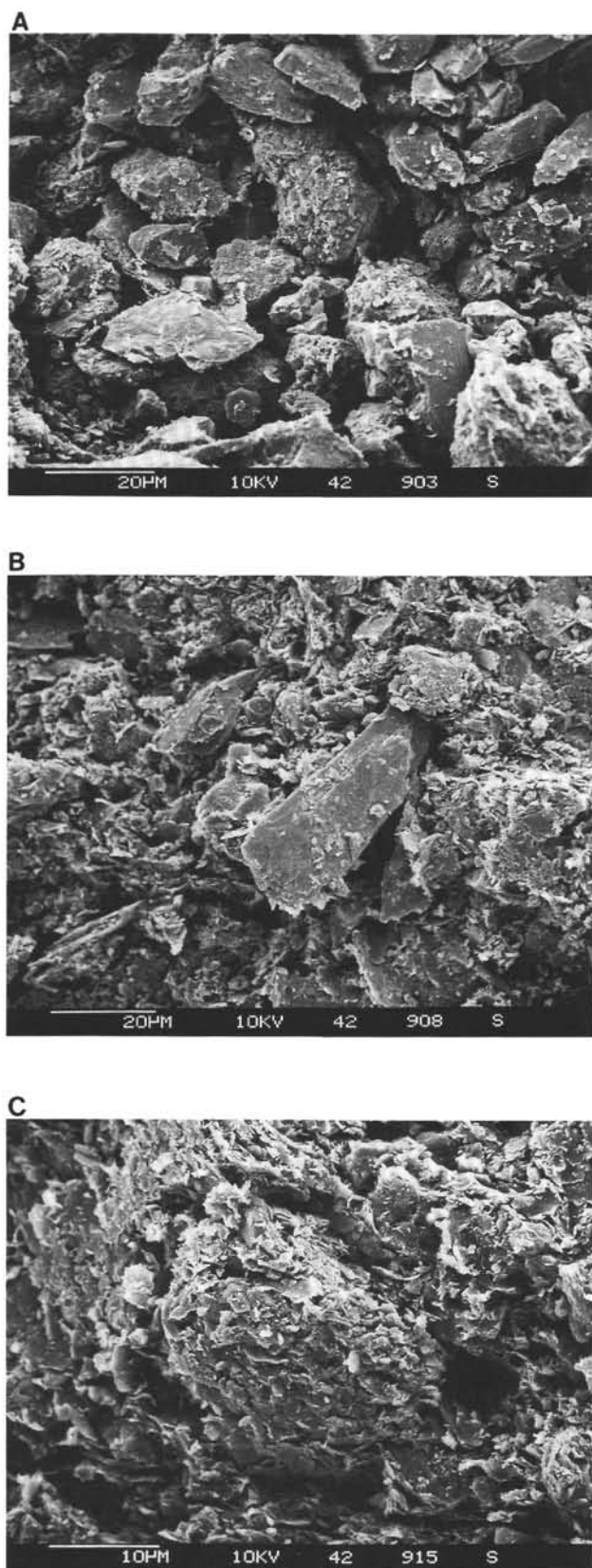
Figure 8. Scanning electron micrographs of sediment from Site 808. **A.** Thin-bedded sands and silt turbidities from lithological Unit IIb, Sample 131-808B-7X-3, 120–140 cm, × 1000. **B.** Silt turbidities and hemipelagic muds from lithological Unit IIc, Sample 131-808C-17R-5, 19–29 cm, × 1000. **C.** Hemipelagic muds from lithological Unit IVa, Sample 131-808C-39R-5, 56–69 cm, × 2000.

It is immediately clear from a compilation of these data (Table 4), that lithological units are clearly distinguished from each other in the compressional field. The angles of internal friction decrease with depth, as expected from the depth-dependent increase in plasticity. An opposite trend seems to prevail in the extensional field, but due to the scarcity of data, it is not possible to quantify this observation. A comparison of results from compressional and extensional triaxial testing shows that angles of internal friction are generally higher in extension, as compared to compression. This difference is well developed in clays of intermediate plasticity in lithological Unit IIc, but less clear in silts from lithological Unit IIb. This observation suggests, as already noted in the oedometer tests, that results from tests on horizontally cut samples are influenced by sample relaxation in the core liner parallel to the core axis.

CONCLUSION

The shipboard classification of lithologic units in Site 808 corresponds significantly with shore-based determined geotechnical index properties, consolidation, and shear strength properties. Thin bedded sands and silt turbidities of lithological Unit IIb are geotechnically characterized as clays of weak plasticity; silt turbidities and hemipelagic muds of lithological Unit IIc as clays of intermediate plasticity; and hemipelagic muds, ashs, and tuffs of lithological Unit IVa as clays of high plasticity.

It has been observed especially that samples of weak plasticity are very sensitive to conservation procedures and handling during and after shipboard sampling. It was possible to determine relaxation processes between shipboard sampling and shore-based testing in silty turbidities from lithological Unit IIb. The impact of relaxation on the results of oedometer as well as triaxial testing could not be quantitatively evaluated. Future sampling for mechanical interpretations of the kind described above should therefore be carried out with extreme care, possibly with the aid of new conservation techniques, e.g., as suggested by Goldscheider and Scherzinger (1991).

Regardless of this limitation, all tests performed provided consistent and clear results to define the mechanical state of sediments from Site 808. The degree of compaction was generally higher than expected from the present vertical sediment overburden. To quantify this overcompaction, the parameter overloading ratio OLR was introduced. OLR increases steadily down to 671.2 mbsf, the maximum depth sampled. Considering the higher OLR values in the horizontal direction and assuming that geostatic overburden has not been higher in the past, the overcompaction measured can only be attributed to the impact of lateral loading in the frontal part of the Nankai accretionary prism.

The anisotropy found in consolidation behavior could also be found in the triaxial stress strain behavior. Sediment stiffness and strength as well as yield limit are higher in horizontal direction. A reconstruction of actual yield loci for sediments of lithological Unit IIb (Fig. 12A) and Unit IIc (Fig 12B) based on all experimentally determined yield points clearly shows that a rotation of both yield loci away from the geostatic NC state into the extensional stress field has occurred. It can be seen that the axes of symmetry of the yield curves synchronize with the stress path 2, which results from large extensional loading, starting from a geostatic stress state given by the actual sediment overburden. This proves that the measured anisotropic mechanical properties as well as the enhanced degree of compaction of Site 808 sediments are a direct consequence of lateral loading due to thrusting.

Beyond this qualitative statement, quantitative information can be given about the in-situ stress regime using the graphical evaluation method represented in Figure 6. By it, Figure 12A provides an actual stress condition of $\sigma_v' = 1.48$ MPa/$\sigma_h' = 1.92$ MPa at a depth of 173.0 mbsf (Unit IIb), Figure 12B of $\sigma_v' = 4.33$ MPa/$\sigma_h' = 8.23$ MPa at a depth of 458.3 mbsf (Unit IIc) with resultant coefficients of lateral stress of $K = 1.3$ and $K = 1.9$, respectively.
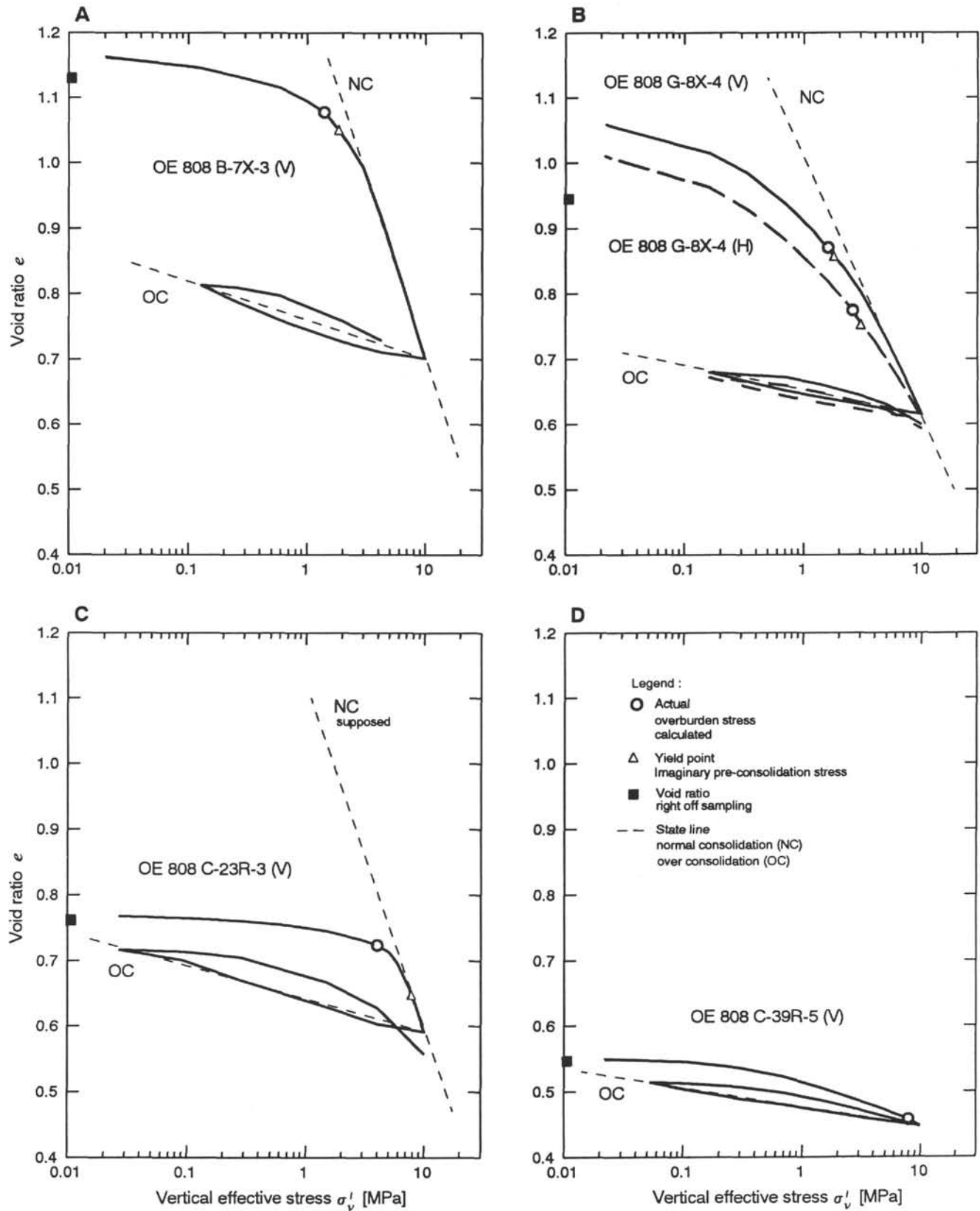
Figure 9. Results of oedometer tests. Compression plane. Semi-logarithmic plot of void ratio vs. effective stress. **A.** Sample 131-808B-7X-3, 120–140 cm (173.0 mbsf). **B.** Sample 131-808G-8X-4, 129–141 cm (198.7 mbsf). **C.** Sample 131-808C-23R-3, 2–14 cm (514.0 mbsf). **D.** Sample 131-808C-39R-5, 56–69 cm (671.2 mbsf).
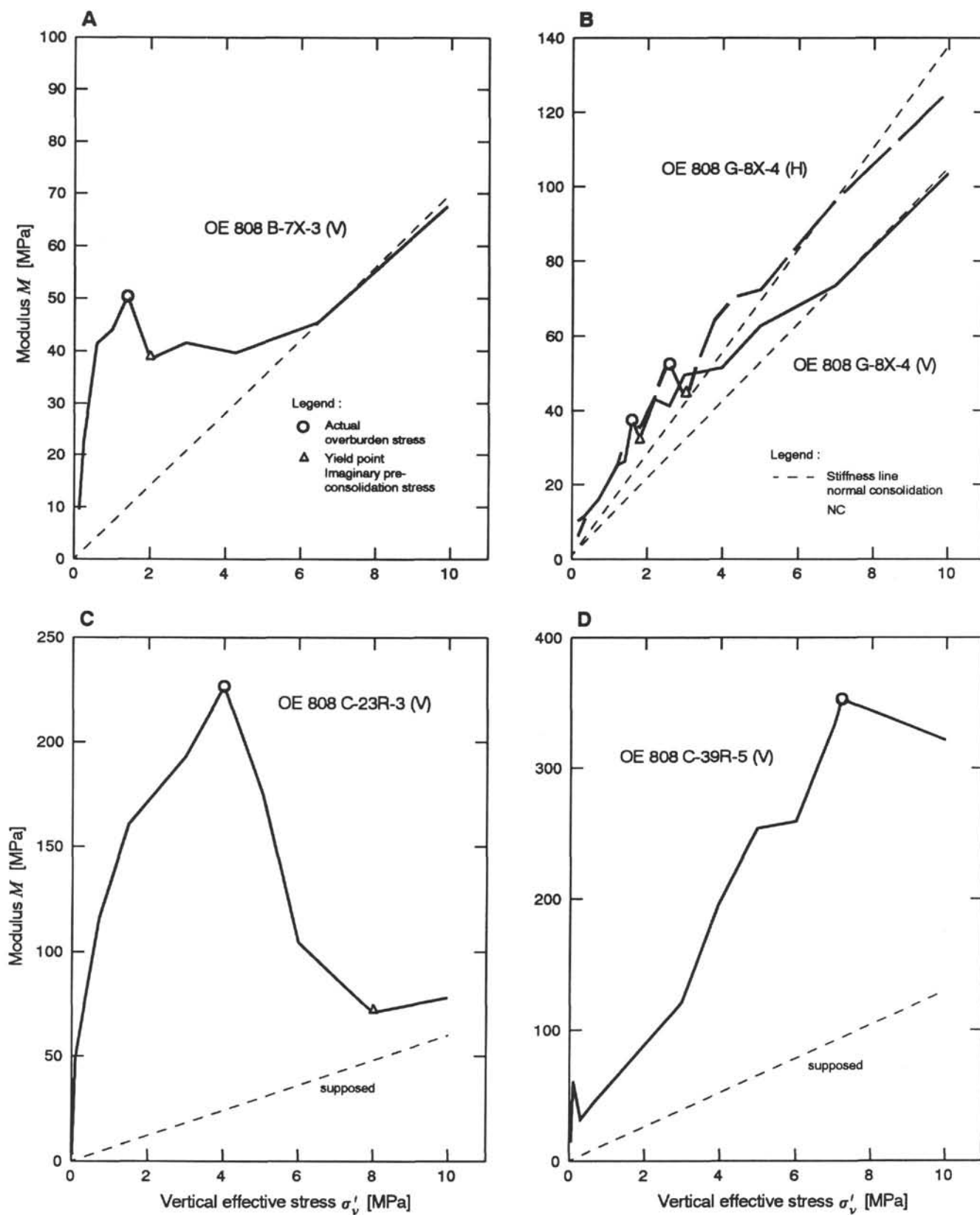
Figure 10. Results of oedometer tests. Development of sediment stiffness. Arithmetic plot of tangent modulus vs. effective vertical stress. **A.** Sample 131-808B-7X-3, 120–140 cm (173.0 mbsf). **B.** Sample 131-808G-8X-4, 129–141 cm (198.7 mbsf). **C.** Sample 131-808C-23R-3, 2–14 cm (514.0 mbsf). **D.** Sample 131-808C-39R-5, 56–69 cm (671.2 mbsf).

REFERENCES*

Barden, L., and Sides, G.R., 1971. Sample disturbance in the investigation of clay structure. *Geotechnique*, 21:211–222.

Berre, T., 1985. *Suggested International Code of Soil Engineering Practice for Triaxial Compression Tests:* NGI (Oslo).

Casagrande, A., 1936. Determination of preconsolidation load and its practical significance. *Proc. 1st Conf. Soil Mech. Found. Eng.* (Vol. 3). Am. Soc. Civ. Eng., 60–64.

————, 1948. Classification and identification of soils. *Trans. Am. Soc. Civ. Eng.*, 113:901–992.

Das, B.M., 1985. *Advanced Soil Mechanics:* New York (McGraw-Hill).

DIN 18 122, 1976. (German Standard) *Testing Procedures and Testing Equipment: Liquid and Plastic Limit.*

DIN 18 123, 1983. (German Standard) *Testing Procedures and Apparatus: Determination of Grain-size Distribution.*

Goldscheider, M., and Scherzinger, T., 1991. Laboratory tests on the soft clayey soil of an old city. *Proc. X Europ. Conf. Soil. Mech. Found. Eng.*, Firenze.

Graham, J., Noonan, M.L., and Lew, K.V., 1983. Yield states and stress-strain relationship in a natural plastic clay. *Can. Geotech. J.*, 20:502–516.

Janbu, N., Tokheim, O., and Sennest, K., 1981. Consolidation test with continuous loading. *Proc. X Int. Conf. Soil. Mech. Found. Eng.*, Stockholm (Vol. 1), 645–654.

Mesri, G., and Choi, Y.K., 1985. The uniqueness of the end-of-primary (EOP) void ratio—effective stress relationship. *Proc. IX Int. Conf. Soil. Mech. Found. Eng.*, San Francisco (Vol. 2), 587–590.

Parry, R.H.G., and Nadarajam, V., 1974. Observations on laboratory prepared lightly overconsolidated specimens of kaolin. *Geotechnique*, 24:345–357.

Roscoe, K.M., Schofield, A.N., and Worth, C.P., 1958. On the yielding of soils. *Geotechnique*, 8:22–52.

Taira, A., Hill, I., Firth, J., Berner, U., Brückmann, W., Byrne, T., Chabernaud, T., Fisher, A., Foucher, J.-P., Gamo, T., Gieskes, J., Hyndman, R., Karig, D., Kastner, M., Kato, Y., Lallement, S., Lu, R., Maltman, A., Moore, G., Moran, K., Olaffson, G., Owens, W., Pickering, K., Siena, F., Taylor, E., Underwood, M., Wilkinson, C., Yamano, M., and Zhang, J., 1992. Sediment deformation and hydrogeology of the Nankai accretionary prism: synthesis of shipboard results of ODP Leg 131. *Earth Planet. Sci. Lett.*, 109:431–450.

Topolnicki, M., 1987. Observed stress-strain behavior of remoulded saturated clay and examination of two constitutive models. *Veroff. Inst. Bodenmech. Felsmech. Univ. Karlsruhe*, H. 107.

Vardoulakis, I., 1979. Bifurcation analysis of the triaxial test on sand samples. *Acta Mech.*, 32:35–54.

Wood, D.M., 1990. *Soil Behaviour and Critical State Soil Mechanics:* Cambridge (Cambridge Univ. Press.).

*Abbreviations for names of organizations and publication titles in ODP reference lists follow the style given in *Chemical Abstracts Service Source Index* (published by American Chemical Society).

Table 3. Data summary of oedometer tests.

Test no.	Depth (mbsf)	Compression index (NC-state) C_c	Swelling index (OC-state) C_s	Overburden stress $\sigma_{v\,act}'$ (MPa)		Yield point $\sigma_{v\,im}'$ (MPa)	Over-loading ratio (OLR)
				calculated	from M vs.σ_v' plot (Fig. 10)		
OE 808B-7X-3 (V)	173.0	0.58	0.059	1.48	1.47	2.0	1.36
OE 808G-8X-4 (V)	198.7	0.37	0.032	1.69	1.60	1.87	1.17
OE 808G-8X-4 (H)		0.29	0.038	[a](0.76)	(1.87)	3.07	1.64
OE 808C-23R-3 (V)	514.0	[b]0.57	0.048	4.89	4.00	8.00	2.00
OE 808C-39R-5 (V)	671.2	[b]0.095	0.029	6.49	7.20	Out of range	–

[a] Horizontal stress (determined by $(1-\sin\varphi')\,\sigma_v'$).
[b] Normally consolidated state not reached.

Table 4. Shear strength parameters (NC state).

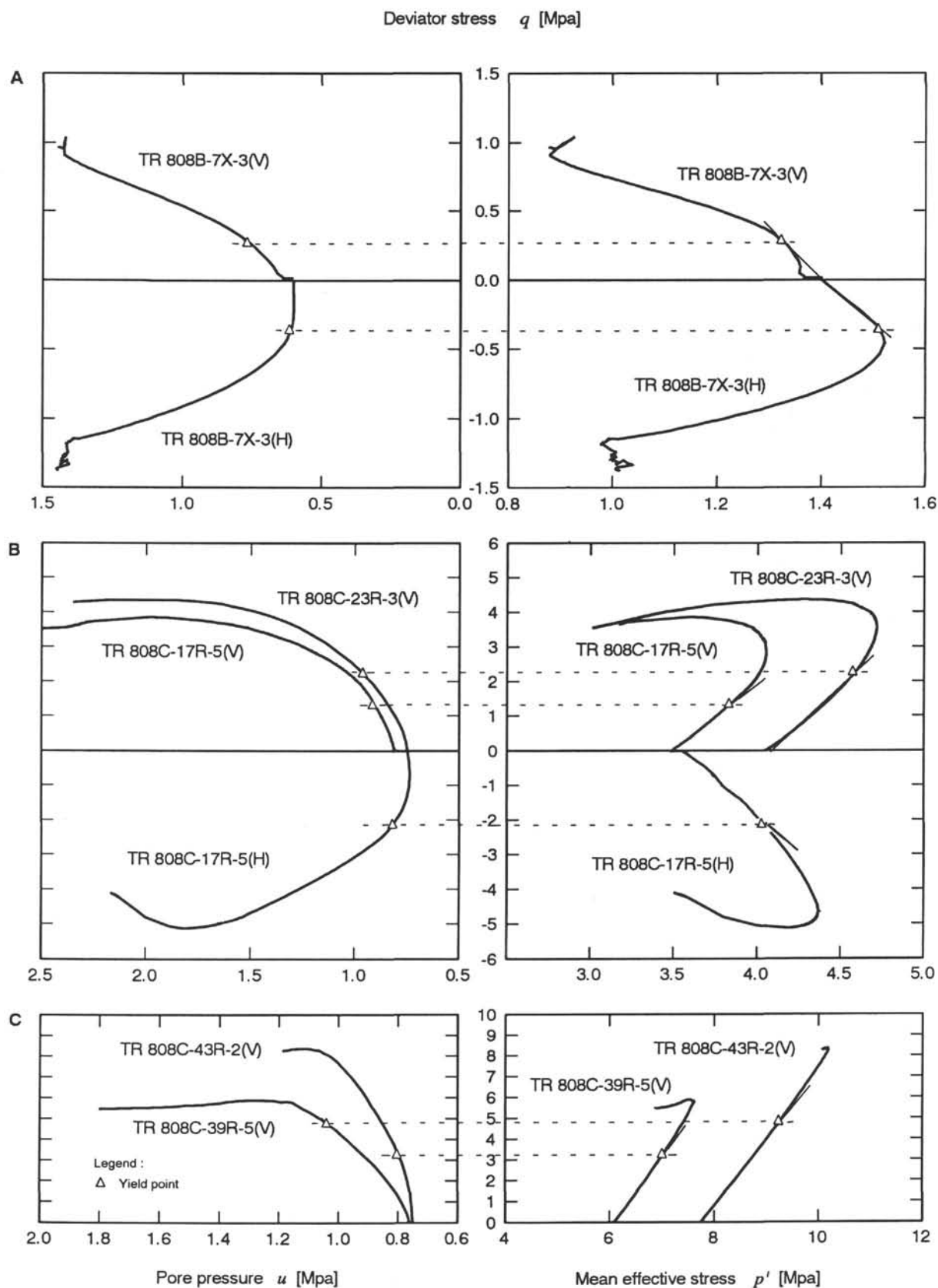| Lithological units	Angle of internal friction	
	Compression φ_c' (°)	Extension φ_E' (°)
IIb	27.0	28.5
IIc	25.5	29.0
IVa	20.8	

Figure 11. Results of undrained triaxial tests (CIUC). Deviator stress vs. pore pressure and deviator stress vs. mean effective stress (Cambridge stress field). **A.** Sample 131-808B-7X-3, 120–140 cm (173.0 mbsf). **B.** Sample 131-808C-17R-5, 19–29 cm (458.3 mbsf) and Sample 131-808C-23R-3, 2–14 cm (514.0 mbsf). **C.** Sample 131-808C-39R-5, 56–69 cm (671.2 mbsf) and Sample 131-808C-43R-2, 18–31 cm (704.9 mbsf).
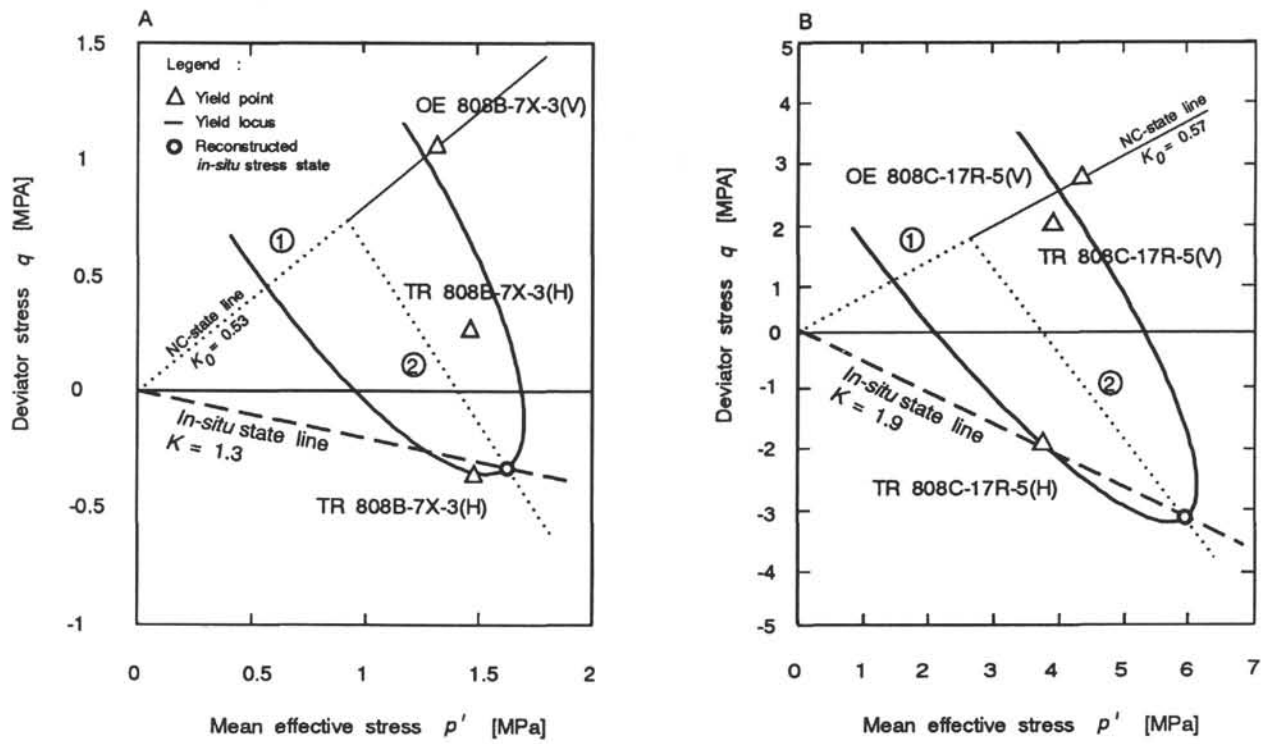
Figure 12. Evaluation of the yield loci and reconstruction of the in-situ stress state for accreted sediment from site 808. Deviator stress vs. mean effective stress (Cambridge stress field). **A.** Lithological Unit IIb. **B.** Lithological Unit IIc.